APL Energy

RESEARCH ARTICLE | APRIL 02 2024

Directed high-energy infrared laser beams for photovoltaic generation of electric power at remote locations

Richard Soref ; Francesco De Leonardis ; Gerard Daligou ; Oussama Moutanabbir

Check for updates

APL Energy 2, 026101 (2024)
https://doi.org/10.1063/5.0197277

View Online
Export Citation

17 May 2024 18:09:56

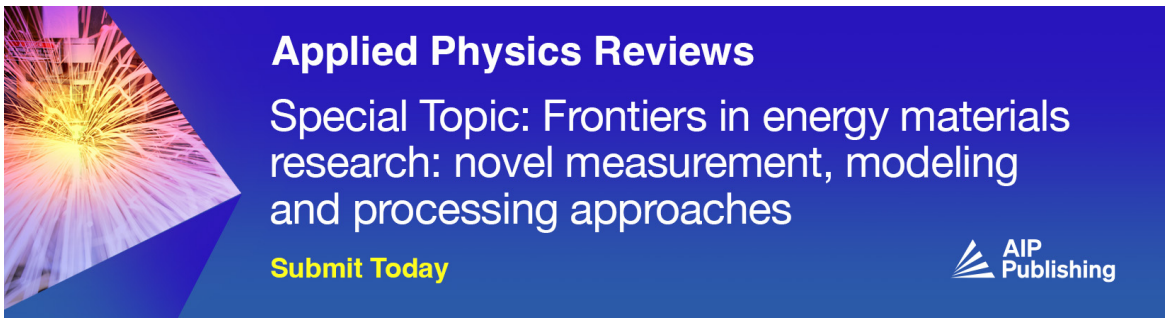

AIP Publishing

APL Energy ARTICLE pubs.aip.org/aip/ape

Directed high-energy infrared laser beams for photovoltaic generation of electric power at remote locations

Cite as: APL Energy 2, 026101 (2024); doi: 10.1063/5.0197277
Submitted: 12 January 2024 • Accepted: 18 March 2024 •
Published Online: 2 April 2024

View Online Export Citation CrossMark

Richard Soref,[1,a)] Francesco De Leonardis,[2] Gerard Daligou,[3] and Oussama Moutanabbir[3]

AFFILIATIONS

[1] Engineering Department, University of Massachusetts at Boston, Boston, Massachusetts 02125, USA
[2] Department of Electrical and Information Engineering, Politecnico di Bari, Bari, Italy
[3] Department of Engineering Physics, École Polyechnique de Montréal, Montréal, Québec H3T 1J4, Canada

[a)] Author to whom correspondence should be addressed: richard.soref@umb.edu

ABSTRACT

Transferring energy without transferring mass is a powerful paradigm to address the challenges faced when the access to, or the deployment of, the infrastructure for energy conversion is locally impossible or impractical. Laser beaming holds the promise of effectively implementing this paradigm. With this perspective, this work evaluates the optical-to-electrical power conversion that is created when a collimated laser beam illuminates a silicon photovoltaic solar cell that is located kilometers away from the laser. The laser is a CW high-energy Yb-doped fiber laser emitting at a center wavelength of 1075 nm with ~1 m^2 of effective beam area. For 20 kW illumination of a solar panel having 0.6 m^2 of area, optical simulations and thermal simulations indicate an electrical output power of 3000 W at a panel temperature of 550 K. Our investigations show that thermo-radiative cells are rather inefficient. In contrast, an optimized approach to harvest laser energy is achieved by using a hybrid module consisting of a photovoltaic cell and a thermoelectric generator. Finally, practical considerations related to infrared power beaming are discussed and its potential applications are outlined.

© 2024 Author(s). All article content, except where otherwise noted, is licensed under a Creative Commons Attribution (CC BY) license (https://creativecommons.org/licenses/by/4.0/). https://doi.org/10.1063/5.0197277

17 May 2024 18:09:56

I. INTRODUCTION

Laser power converters for power-by-light and optical-wireless have been discussed in the literature,[1,2] and this paper addresses the aspects of (1) directed laser beams enabling electric-power generation at remote locations and (2) cases in which a very-high-power aimed beam travels through the ambient atmosphere to reach a targeted optical-to-electric (OE) converter that is located, for example, kilometers away from the laser, a remote location that is typically "off the grid." To leverage the atmospheric transparency windows, we are considering infrared lasers here, not the visible ones.

The thesis of this paper is twofold: (1) powerful lasers have dual use for civilian and military purposes and (2) the well-known silicon solar cell can also have dual use for harvesting laser beams as well as sunlight.

Using modeling, we have considered both thermo-radiative (TR) and photovoltaic (PV) receivers, and we find that the TR approach is much less efficient than PV in converting laser power into electric power. Our thermal simulations of the silicon solar PV cell show unavoidable heating of the cell, which is traditionally viewed as undesirable, but which we find beneficial in the laser case because the optimized electrical output occurs at a PV body temperature well above room temperature, such as 550 K, as detailed in Sec. XII. We have also investigated the combination of a PV cell with a thermoelectric generator (TEG) whose large area matches the area of the PV cell. Both PV and TEG are silicon-based and manufacturable. This PV + TEG hybrid provides electric power from both PV and TEG. The rear face of the TEG is ambient-cooled, while the front TEG face thermally contacts the "heated" PV, thus providing a desired temperature-drop across TEG. We thus recommend PV + TEG as an optimized approach to directed-laser OE.

© Author(s) 2024

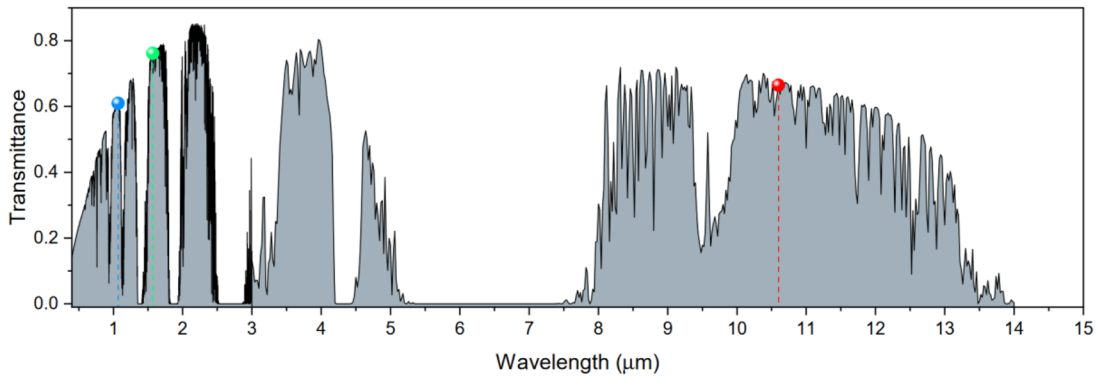

FIG. 1. Transmittance spectrum of the earth's atmosphere at sea level.[11] The dots indicate the wavelengths of different lasers that can be considered for energy beaming: 1075, 1567, and 10 600 nm corresponding to high atmospheric transmittance.

Our approach utilizes ultra-high-power (UHP) lasers, whose optical output is 10 kW or more. In the UHP case, there is an interplay or trade-off between the PV receiver spectral absorption, the temperature rise in the receiver, and the receiver's OE conversion efficiency that decreases with increasing PV temperature, but a decrease that is not large enough to prevent practical applications. Optical engineering and thermal engineering studies here allow us to select the optimum range of laser beam power. Optimizing the receiver load resistance is also important.

The sections of this paper cover UHP beaming lasers, potential and significant applications of beaming, silicon "solar" PV near-infrared application, PV conversion details, thermal and optical simulation results, benefits of using multi-solar-cell modules (panels), solar PV combined with group-IV TEG for high performance harvesting, analysis of the TR approach, and system costs-and-benefits.

II. UHP LASER FOR BEAMING

We are considering infrared lasers rather than the ones that emit visible light, and we choose laser wavelengths corresponding to an atmospheric transparency window. Four relevant lasers within the near infrared, shortwave infrared, and longwave infrared satisfy this condition. 20 kW CW longwave infrared CO_2 lasers at the 10.6 μm wavelength are already commercially available for the present beaming applications.[3] For the near infrared, there are commercial solid-state diode lasers whose output is anywhere within the 900–1080 nm wavelength range and where 10 kW CW (or higher) output is available from several vendors.[4–6] Arrays of diodes are placed upon a bar, and, then, bars are stacked in several layers. The beams from stacked bars are then combined, giving a spot-focus with a condenser lens. To that spot, we would add a beam-collimating lens for our case. We also select two of these lasers, the 900 nm and the 1000 nm versions as having the highest transmission through the atmosphere. In addition, manufacturers have created an Er-doped fiber laser emitting at the 1567 nm wavelength, and this can be purchased in the 4 kW CW version.[7] Finally, we come to the most important or primary laser of this investigation, which is the Yb-doped fiber laser that emits typically over a 1070–1080 nm band. Government agencies and contractors have developed UHP 50–300 kW embodiments of these lasers for military applications;[8] but we are recommending here that such lasers have also potential applications in energy beaming. There is already a report of a 100 kW Yb fiber laser configured for cutting and welding applications.[9] And not least, there are 20 kW CW Yb-doped fiber lasers available commercially.[10] In this paper, our simulations cover the 0.1–50 kW laser power range, and we find that laser power around 20 kW is optimal for energy harvesting.

Turning to the atmospheric transmission of laser beams, Fig. 1 illustrates the high transmission of 1075, 1567, and 10 600 nm "directed-laser illuminators" by dots placed upon the atmospheric transmission spectrum.

We shall assume that the laser is in CW operation. Pulsed laser emission is feasible but is considered not optimum for electric power generation.

III. PROPOSED APPLICATIONS AND SCENARIOS

Using a distant target-mounted PV cell in conjunction with a powerful, pointed, laser beam can have various practical applications, especially in remote or off-grid areas. The following is a list of potential applications for the electric power generated by this proposed system:

1. Power generation for remote monitoring: This PV system would power remote equipment such as weather stations, wildlife cameras, or environmental sensors, in areas where access to the electrical grid is not feasible.
2. Wireless communication: The generated electricity can be used to power radio or satellite communication equipment, enabling communication in isolated areas, for example, during emergencies.
3. Renewable energy for off-grid homes and remote research stations: In unpopulated or remote areas with limited-or-no sunlight, PV cells powered by a distant laser can serve as

17 May 2024 18:09:56

© Author(s) 2024

a source of renewable energy for off-grid homes and cabins, providing electricity for lighting, appliances, and charging devices. Scientific research stations in remote locations with limited-or-no sunlight can benefit from the PV system to power scientific instruments, computers, and communication devices.

4. Pumping water for remote irrigation: The electricity generated can be used for pumping water in agricultural applications, providing a sustainable source of water for irrigation.
5. Emergency power for disaster relief: PV cells with a distant laser source can be deployed in disaster-stricken areas to provide emergency power for lighting, medical equipment, and communication devices.
6. Wildlife conservation efforts: The technology can support wildlife conservation efforts by powering cameras and tracking devices in remote regions.
7. Surveillance: Here, the PV cells could be used for long-range surveillance and security applications, enabling continuous operation of cameras and sensors in strategic locations.
8. Remote power for space probes: In space exploration, PV cells could be used to power instruments and communication systems on unmanned spacecraft sent to distant planets or celestial bodies.
9. Remote powering of aircraft: Assuming that the beam-pointer tracks the aircraft in real time, the aircraft-mounted PV can power that airplane. This application overlaps the DARPA Persistent Optical Wireless Energy Relay program announced in 2023, a program in which the goal is to mount the UHP laser on a flying aircraft and to beam that power over distances up to 200 km to other flying aircraft.
10. Environmental monitoring stations: PV-powered stations can continuously monitor environmental conditions in remote areas, helping to collect valuable data for research and conservation efforts.
11. Mining and resource extraction: In remote mining or resource extraction operations, PV cells can provide electricity for essential equipment and/or communication systems.

When implementing these systems, it is important to consider factors such as laser safety, PV opto-electric efficiency, local regulations, environmental considerations, and the costs of deploying and maintaining the system. Atmospheric issues to contend with include thermal blooming of the beam, atmospheric turbulence, smog, fog, smoke, and rain. As indicated, the laser can be on earth, shipborne, airborne, or space-borne.

IV. PHOTOVOLTAIC OE CONVERTERS OF LASER ENERGY

We have investigated the PV approach, the hybrid PV-and-TEG approach, and the thermo-radiative (TR) diode approach to OE conversion, detailed as follows: We are proposing direct illumination of the PV diode's input face by the laser as being the most effective situation. One can also envision an indirect PV approach in which a sheet or thick layer of absorber–emitter (a–e) material is placed in front of the PV diode's front side in order to absorb laser light in the a–e, thereby heating it, and thereby creating a blackbody emitter at some high temperature that then radiates to the "nearby" PV diode. However, even if we assume that the PV absorbs a large portion of the blackbody radiation spectrum, this a–e scenario is not optimum for OE conversion because the blackbody power density in W/m^2 (averaged over the absorbed spectral region) is a smaller power density than that supplied by the UHP laser, even for high blackbody temperatures such as 1000 or 1200 K. In summary, the direct PV illumination has obviously higher efficiency.

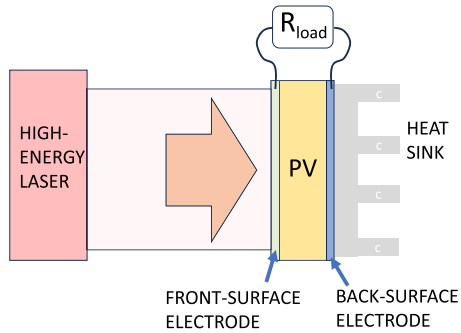

FIG. 2. Schematic view of laser power beaming by means of a PV cell.

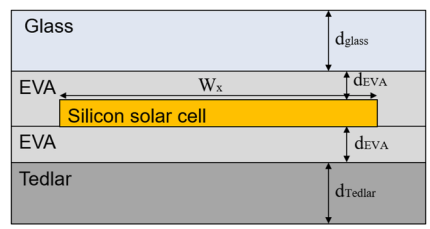

FIG. 3. Cross section view of the high-performance cost-effective silicon solar cell. Relevant parameters and materials are indicated. A standard commercial cell has an area of 15.6 × 15.6 cm^2.

V. SILICON SOLAR CELL FOR NIR BEAMED OE

The OE conversions of the 1570 and 10 600 mm UHP laser beams will be quantified in a subsequent study, while in this work, we shall examine the near-infrared cases. Considering PV semiconductors generally, PV theory indicates that the optimum bandgap wavelength λ_g of the PV diode is slightly longer than the laser wavelength. For the 900–1000 and 1075 nm UHP lasers, it is fortuitous that the extremely familiar silicon PV solar cell (λ_g = 1107 nm at 300 K) satisfies this relation. Hence, efficient OE conversion is expected, as we quantify.

The direct-illumination approach is shown in Fig. 2, and here, it is important to remove heat from the PV, which is done to some extent by the metal heat sink at the rear, which works in the ambient air. There is also air convention cooling at the front, and the cell emits gray body radiation with 0.8 emissivity. Figure 3 presents the cross section view of the most popular solar cell.[12,13] It is seen that the absorption of the laser beam takes place across the 180 μm (or 500 μm) thickness of the cell.

17 May 2024 18:09:56

© Author(s) 2024

VI. THERMAL ANALYSIS OF THE Si PV APPROACH

In this section, the thermal physics model of the laser heating of PV structures is presented. Here, the purpose is to describe the main effects in order to ascertain the PV figure of merit as a function of PV body temperature, induced by laser illuminations.

The PV is irradiated by means of a laser spot having a size opportunely chosen to induce the heating effect over most of the PV cell area. In this context, the three-dimensional energy equation of the PV structure is expressed as follows:

$$\rho C_p \frac{\partial T}{\partial t} + \rho C_p \mathbf{u} \cdot \nabla T - \nabla(k \nabla T) = Q_{laser} - Q_{PV}, \tag{1}$$

where C_p is the specific heat capacity; k is the thermal conductivity; ρ is the density; and T, Q_{laser}, and Q_{PV} represent the temperature, the heat source induced by the laser-energy absorption, and the electrical power density generated by the photovoltaic volume, respectively. Equation (1) clearly evidences that the temperature T of the system is related to the difference between the heat source Q_{laser} generated by the absorption of the laser and the internal heat sink induced by Q_{PV}. According to the Beer–Lambert law, the heat source in each layer ($Q_{laser}^{(i)}$) is given by

$$Q_{laser}^{(i)} = Flux^{(i-1)} \cdot \alpha_i \cdot e^{(-\alpha_i \cdot z)}, \tag{2}$$

where the subscript i = 1, 2, 3, 4, 5 stands for glass (i = 1), EVA (i = 2 and 4), Si (i = 3), and Tedlar (i = 5) and α_i is the absorption coefficient in the ith layer. The term z represents the coordinate in the vertical direction of the PV cell. Since the absorption coefficient of the silicon is dominant, during the entire laser illumination, the instantaneous energy of the laser beam is mainly absorbed by the silicon layer (see Fig. 3) and is converted into a thermal source.

Moreover, the silicon loss coefficient $\alpha(\lambda, T)$, dependent on the temperature and wavelength, is calculated as[14]

$$\alpha(\lambda, T) = \sum_{\substack{i=1,2\\ j=1,2}} C_i A_j \left\{ \frac{\left[\hbar\omega - E_{gj}(T) + E_{pi}\right]^2}{\left[e^{\frac{E_{pi}}{k_{BT}}} - 1\right]} + \frac{\left[\hbar\omega - E_{gj}(T) - E_{pi}\right]^2}{\left[1 - e^{\frac{-E_{pi}}{k_{BT}}}\right]} \right\} + A_d\left(\hbar\omega - E_{gd}(T)\right)^{1/2}, \tag{3}$$

where the indirect $[E_{gj}(T)]$ and direct $[E_{gd}(T)]$ bandgap energies are expressed as a function of temperature by means of the Varshni equations.[14] Moreover, the values of the phonon energies (E_{pi}) and of the fitting constants C_i, A_j, and A_d are listed in Table I of Ref. 14.

By assuming that the laser beam has a Gaussian spatial distribution, the laser flux in the top is given by

$$Flux = (1 - R)\frac{2 \cdot P_{laser}}{\pi \cdot r_{sp}^2} e^{\left(-2\frac{(x - x_{focus})^2 + (y - y_{focus})^2}{r_{sp}^2}\right)}, \tag{4}$$

where R is the reflectivity at the top glass surface, P_{laser} is the input laser power, and r_{sp} represents the laser spot radius. The terms x and y are the coordinates in the xy plane of the PV cell, and x_{focus} and y_{focus} represent the spot's center point.

In order to realize a self-consistent model, the internal heat sink Q_{PV} is calculated as $Q_{PV} = \eta \times Q_{laser}^{(Si)}$, where η represents the PV conversion efficiency for monochromatic illumination. In this context, Green *et al.*[15] have experimentally demonstrated conversion efficiency in silicon cells above 45%, under illumination equivalent to monochromatic light intensities of about 1 W/cm^2. In particular, efficiencies close to 40% were recorded for light at the 1064 nm wavelength as emitted by neodymium-doped yttrium-aluminum garnet (Nd:YAG) lasers. In this sense, we think that Green's theoretical derivation (summarized in the following) offers good agreement with the experimental data and can be well integrated with the 3D thermal simulations. Thus, the conversion efficiency for monochromatic illumination is evaluated as

$$\eta = \frac{J(V)V}{Flux}, \tag{5}$$

where the density current depending on the voltage V is calculated as

$$J(V) = q\int_{E_g}^{\infty} a(E) n_{in}(E) dE - q\frac{2\pi\Delta\Omega}{h^3 c_0^{2ERE}} \int_{E_g}^{\infty} a(E) \frac{E^2}{\left[e^{\left(\frac{E-qV}{kT}\right)} - 1\right]} dE, \tag{6}$$

where $\Delta\Omega$ indicates the solid angle. The first term in Eq. (6) is the absorbed photon flux from the laser beam. The photon-energy dependent coefficient $a(E)$ is the PV absorbance, and $n_{in}(E)$ represents the input photon flux density, assumed to have a Gaussian distribution around the central photon energy emission with FWHM $\delta E = 2\pi c_0 \delta\lambda/\lambda^2$, where $\delta\lambda$ is the emission bandwidth. Finally, the term *ERE* (external radiative efficiency) represents the fraction of all photon losses from the device (i.e., nonradiative recombination).

VII. RESULTS OF THERMAL AND OPTICAL SIMULATIONS

We investigated the thermal aspects of the laser illumination of the silicon PV sketched in Fig. 3, and we modeled the laser heating using the finite element method (COMSOL Multiphysics) models. We performed 3D simulations where the heat-transfer-in-solids model is coupled together with the model of the conversion efficiency [see Eqs. (5) and (6)] in an integrated approach to include in the thermal simulations [see Eq. (1)] the internal heat-sink effect induced by the electrical power generation. Some main experimental parameters, such as the laser power, laser spot size, and the thickness of the silicon cell, are discussed in detail to investigate their influence on both the temperature distribution and the PV figure of merit.

According to Fig. 3, we targeted the silicon PV having $W_x \times W_y$ = 15.6 × 15.6 cm^2, d_{glass} = 3 mm, d_{EVA} = 0.4 mm, and d_{Tedlar} = 0.5 mm. Moreover, in the following analysis, we assumed the silicon layer thickness, d_{Si}, of 180 μm and 500 μm, and the wavelength emission of the UHP laser λ = 1075 nm, with the emission bandwidth $\delta\lambda$ = 10 nm.

17 May 2024 18:09:56

© Author(s) 2024

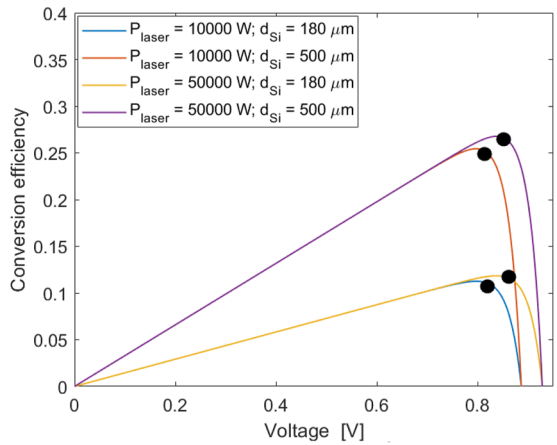

FIG. 4. Conversion efficiency as a function of voltage, for laser power values of 10 000 and 50 000 W and d_{Si} = 180 and 500 μm, respectively. In the simulations, the laser emission wavelength and the laser spot radius (r_{sp}) are 1075 nm and 80 cm, respectively. The operative temperature is forced at 300 K.

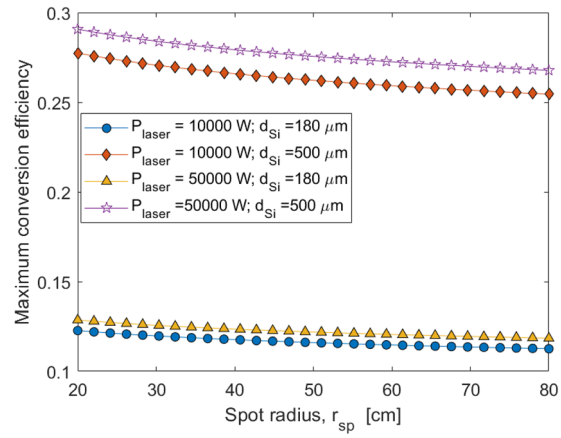

FIG. 5. Maximum conversion efficiency as a function of laser spot radius, for laser power values of 10 000 and 50 000 W and d_{Si} = 180 and 500 μm, respectively. In the simulations, the laser wavelength emission and the emission bandwidth are 1075 and 10 nm, respectively. The operative temperature is forced at 300 K.

As a first step, we performed parametric simulations based on Eqs. (5) and (6) in order to evaluate the influence of the design parameters on the conversion efficiency. In this context, our investigations are plotted in Figs. 4 and 5. In particular, Fig. 4 shows the conversion efficiency as a function of voltage, for different values of the laser power, where the operative temperature is controlled at 300 K. As is well-known, the output electrical power density, $J(V)V$, must be optimized over V. As a result, the maximum conversion efficiency (at the Maximum Power Point, MPP) is evaluated at the optimum V and is then adopted in the following analysis as the figure of merit. The curves in Fig. 4 clearly indicate that the maximum conversion efficiency increases by increasing d_{Si} from 180 to 500 μm, with a slope $\partial\eta/\partial d_{Si} = 0.000\,441\,8\ \mu\text{m}^{-1}$. Since the operative temperature is forced to 300 K, this trend is essentially depending upon the different values of the PV absorbance. Indeed, because the calculated absorption depth is 940 μm (at 300 K), a larger number of photons are absorbed when d_{Si} is ~500 μm, resulting in a larger generated density current $J(V)$.

Using the optimum V value, we then calculate the maximum conversion efficiency as a function of laser spot radius (r_{sp}), presented in Fig. 5. In this figure, the laser power is assumed as 10 000 or 50 000 W and the operative temperature is controlled to 300 K. Related to the absorbance, a strong linkage of $\eta_{\max}$ to d_{Si} is found in Fig. 5, as it was in Fig. 4. The four curves in Fig. 5 exhibit a modest decrease in $\eta_{\max}$ with increasing spot radius, and the cause of this is the decrease in the Gaussian-distributed photon flux density $n_{in}(E)$ in Eq. (6).

From the plot, we record that the maximum conversion efficiency decreases with increasing spot radius with a slope of $\partial\eta/\partial r_{sp}$ = −0.000 159 8 and −0.000 361 3 cm^{-1} for d_{Si} = 180 and 500 μm, respectively. Moreover, the curves show that $\partial\eta/\partial r_{sp}$ values are weakly dependent upon the level of the laser power.

At this step, we present the heating effect upon the maximum conversion efficiency, by performing 3D simulations integrating Eqs. (3)–(6) in the FEM tool. The material properties used in the thermal simulations are summarized in Table I.

TABLE I. Physical parameters of thermal simulation.

Parameters	Materials			
	Silicon	Glass	EVA	Tedlar
Density (kg/m^3)	2330	2450	950	1200
Thermal conductivity (W/mK)	130	2	0.311	0.15
Heat capacity at constant pressure (J/kg K)	677	500	2090	1250

The conditions considered in the thermal simulations are as follows: (a) the thermophysical parameters of all photovoltaic materials are presumed to be isotropic and independent of temperature, (b) the PV side boundary is considered adiabatic, (c) the initial temperature of the PV structure is equal to the ambient temperature (T_0 = 293 K), (d) the heat flux due to heat losses by radiative and convective heat transfer between the PV and environment is applied to the top and bottom surfaces.

Regarding convection, we have assumed here a passive heat sink at the PV bottom surface, a sink consisting of a fin array that is exposed to the ambient air in order to dissipate heat. Although this convection cooling is helpful, it does not prevent PV temperature rise. If we had imposed, instead of convection, the constraint that the body of the PV converter must always be held at 293 K during the incoming UHP beaming, that would have required considerable *active* heat sinking, which means that electrically powered devices would be deployed: blowers to force air onto the sink, or pumps to send fluids through the sink. Such electric powering would in our view be counter-productive since it would subtract significant power from the "net" electric power generation. For example, it would be

17 May 2024 18:09:56

© Author(s) 2024

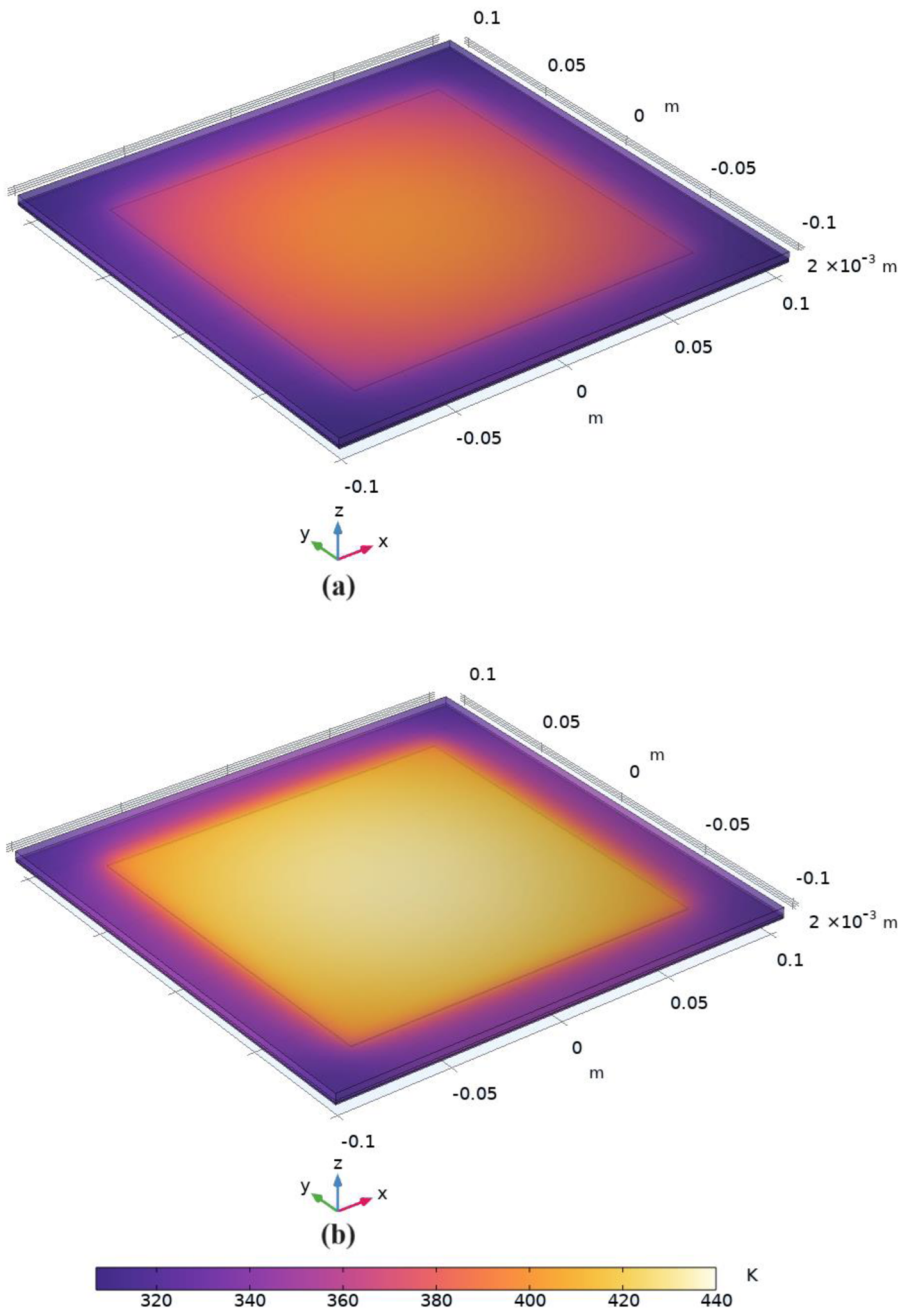

FIG. 6. Temperature distribution in a 156 × 156 mm^2 silicon PV. (a) Laser power 10 000 W and d_{Si} = 180 μm and (b) laser power 10 000 W and d_{Si} = 500 μm. In the simulations, the laser wavelength emission, the emission bandwidth, and the laser spot radius (r_{sp}) are 1075 nm, 10 nm, and 80 cm, respectively.

a formidable electrical task to remove the heat induced by 20 kW of PV-absorbed power.

In this context, the spatial temperature distribution for the laser heating process is shown in Figs. 6(a) and 6(b), for d_{Si} = 180 and 500 μm, respectively. In the simulations, a laser power of 10 000 W has been assumed. The plots clearly indicate that the silicon PV with d_{Si} = 500 μm reaches higher temperature values. This trend can be explained in terms of the absorption depth. When the temperature increases, the silicon absorption increases and then the absorption depth reduces. We record the absorption depth values of 940 μm

17 May 2024 18:09:56

© Author(s) 2024

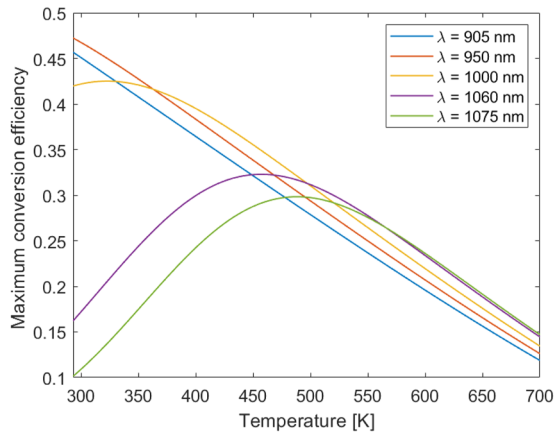

FIG. 7. Maximum conversion efficiency as a function of Si PV body temperature for five laser-emission wavelengths. In these simulations, d_{Si} = 180 μm.

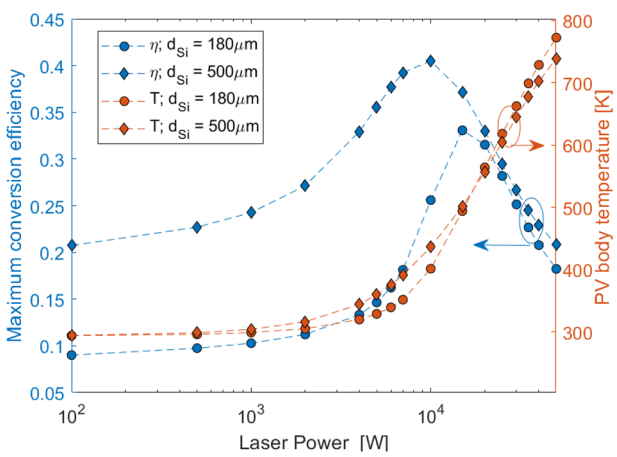

FIG. 8. Maximum conversion efficiency and PV body temperature as a function of laser power, ranging from 100 to 50 000 W, for d_{Si} = 180 and 500 μm. In the simulations, the laser wavelength emission, the emission bandwidth, and the laser spot radius (r_{sp}) are 1075 nm, 10 nm, and 80 cm, respectively.

decreasing to 253 μm when changing the temperature from 300 to 400 K. Under these conditions, the number of absorbed photons is maximized for d_{Si} = 500 μm with respect to the case d_{Si} = 180 μm, inducing a larger heat source term in Eq. (2).

Using Eqs. (2)–(6), and taking into account the increased PV absorption induced by bandgap shrinkage in silicon when the body temperature increases above 293 K, we have plotted in Fig. 7 the resulting conversion efficiency-versus-temperature for incoming laser power at the 905, 950, 1000, 1060, and 1075 nm wavelengths.

Our parametric investigation of the 1075-nm laser heating process is presented in Fig. 8, which shows the maximum conversion efficiency (left axis) and the PV body temperature (right axis) as

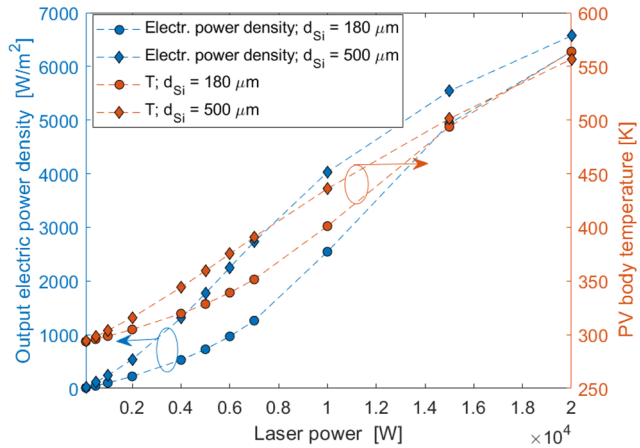

FIG. 9. Output electrical power density and its associated PV body temperature as a function of laser power, ranging from 0 to 20 000 W, for d_{Si} = 180 and 500 μm. In the simulations, the laser wavelength emission, the emission bandwidth, and the laser spot radius (r_{sp}) are 1075 nm, 10 nm, and 80 cm, respectively.

a function of laser power, for d_{Si} = 180 and 500 μm, respectively. In both cases, the maximum conversion efficiency reaches a peak value (η_{peak}), corresponding to a particular value of the laser power (P_{peak}) to which corresponds, in turn, a well-determined heating temperature (T_{peak}).

It is worth outlining that, in our integrated approach, the temperature dependence of the conversion efficiency is taken into account by means of the following main contributions: (i) the density current relationship of Eq. (5), (ii) the absorbance by means of the silicon absorption coefficient [see Eq. (3)], and (iii) the Varshni equation applied to the silicon energy bandgap.[14]

At this point, we will assert that the electrical output power density is the most practical or meaningful figure of merit for this laser beaming, and for that reason, we have simulated the density increase with laser power, as presented in Fig. 9 (left axis) together with the results for the associated PV body temperature (right axis). Both density and temperature increase strongly with beam power. Now, we shall, somewhat arbitrarily, set a limit of 550 K as being the maximum usable operating temperature of the Si PV. With that provision, we have obtained the OE results summarized in Table II for incident laser powers of 10 000, 15 000, 19 013, and 19 388 W.

Regarding the OE figure of merit for Table II, the traditional approach is to use the power conversion efficiency $\eta_{\max}$ at the maximum power point of the conversion device. This merit figure is given by $\eta_{\max} = D_c/D_b$, where we define the beam density $D_b = P_b/A_b$, in which P_b is the input power of the laser beam and A_b is the effective area of the collimated incident laser beam, and where $D_c = P_c/A_c$, in which P_c is the output electric power of the cell and A_c is the area of that cell. We assume a collimated cylindrical laser beam with a Gaussian intensity distribution, for which r_{sp} is the radius where the beam intensity has fallen down to $1/e^2$ of the central beam power. Then, we define the effective area of the beam $A_b = \pi r_e^2$, where r_e is the effective beam-spot radius given by $r_e = r_{sp}/\sqrt{2}$, yielding

17 May 2024 18:09:56

© Author(s) 2024

TABLE II. Summary of results.

Laser power input (W)	Metrics: PV body temperature (K)	Efficiency	Output electric power density (W/m^2)	Output electric power (W) for A = 0.0243 m^2
19 013 (d_{Si} = 180 μm)	550	0.32	6008	146
19 388 (d_{Si} = 500 μm)	550	0.33	6443	157
15 000 (d_{Si} = 180 μm)	501	0.33	4935	120
10 000 (d_{Si} = 500 μm)	436	0.41	4029	98

$A_b = \pi r_{sp}^2/2$. In Table II, the effective area of the Gaussian laser column is one square meter, based upon the beam-column effective radius of 56.6 cm.

In practice, the most important figure of merit is the absolute electric power emerging from the cell, which is $P_c = \eta_{\max} P_b A_c / A_b$. Using the P_c criterion, the electric output power results given in Table II are 146 W (d_{Si} = 180 μm) and 157 W (d_{Si} = 500 μm) for input laser powers of 19 013 and 19 388 W, respectively. These electrical results refer to a solar cell whose area is only 2.4% of the effective area of the incident beam. This immediately indicates that we require larger-area OE converters to achieve larger electrical outputs.

VIII. SOLAR PANEL ESTIMATES

If we now consider a 5 × 5 interconnected array of the above-cited standard cells in order to construct a custom-made solar panel, then the PV area increases to ~0.61 m^2, which is a factor-of-25 enlargement. Taking that panel as the new OE converter, we then propose to use the same 1.0 m^2 effective-area cylindrical laser beam (A_b) to illuminate and flood the panel. The electrical power output P_c scales as the PV area A_c according to the above relation. $P_c = \eta_{\max} P_b A_c / A_b$. One estimate is that P_c will increase by a factor of 25, but a more conservative approach is to say that P_c will be higher by a factor of 15 or 20 because the beam intensity is not constant across its area A_b (nonuniform illumination). In that case, using the factor-of-15 and factor-of-20 predictions, taking the result of 157 W at 500 μm Si PV thickness (550 K PV body) (Table II), we find for the 15 and 20 predictions P_c = 2355 and 3140 W, respectively. Therefore, there appears to be a realistic pathway to 3000 W output for 20 000 W laser input. We should mention that the 32-module array proposed in Fig. 10 appears to give a 28% improvement over the 5 × 5 array.

We considered factors that could limit the performance of a multi-module panel, i.e., arrays such as 5 × 5 or 32 or 6 × 6. Specifically, in Sec. VI, and in Table II, for an individual module, we took into account the external radiative efficiency (ERE), a parameter that accounts for carrier recombination losses. Resistive losses were not included. However, resistive effects in individual solar cells do reduce the fill factor (FF) and then reduce the efficiency of the cell by dissipating power in the resistances. In particular, the most common parasitic resistances are the series resistance and the shunt resistance. In our PV modules, typical values for the

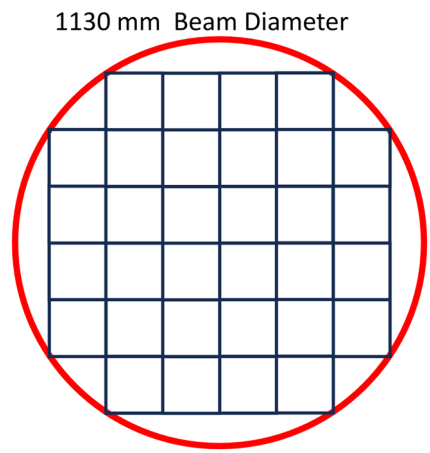

FIG. 10. Schematic drawing of the 32-cell Si PV panel having an area of 0.78 m^2. The array overlap with the laser beam is shown.

area-normalized series resistance are around 0.5 Ω cm^2. By contrast, the values for the shunt resistance are in the MΩ cm^2 range for laboratory-type solar cells and 1000 Ω cm^2 for commercial solar cells. In this context, due to the large area used for one cell (0.0243 m^2), the dominant resistive effect is determined by the series resistance R_{SER}.

To accurately represent our case, we shall make the assumptions d_{Si} = 500 μm, a laser power of 10 000 W, and a PV body temperature of 436 K. Then, we estimate that the series resistance induces an electric power loss of around 52% for the single PV cell. However, considering the load resistance connected to the panel, the resistive effect has a negligible effect on a series-interconnected multi-module panel array. Thus, we propose to connect the entire array in electrical series. The result of this technique is that the series resistance of the panel array containing 25 or 36 solar cells induces a power loss of 2% or 1.44%, respectively. Thus, the overall result of this finding is that ERE remains as the limiting factor for our multi-module PV arrays larger than 5 × 5.

Returning to Fig. 7, in addition to 550 K, there are many practical choices for the 1075-nm laser power and PV operating temperature. Figure 7 also shows that there are additional laser choices for Si-PV harvesting, such as the ~905 nm direct-diode

17 May 2024 18:09:56

© Author(s) 2024

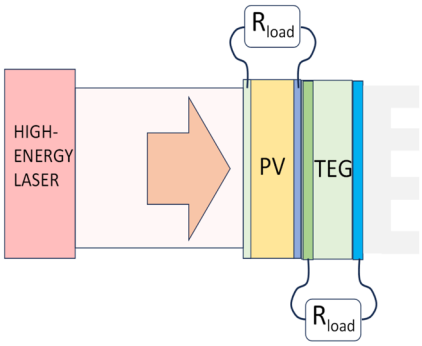

FIG. 11. Schematic drawing of the beam-actuated PV-and-TEG hybrid with combined electrical outputs.

laser mentioned above. Our simulations (not shown here) reveal curves that are very close to those in Fig. 8. In other words, our diode-laser simulations predict that when the 905 nm laser-beam illuminates the above-described solar panel, the resulting electric power outputs will be quite comparable to those for the Yb-fiber laser case.

IX. PV DIODE SUPPLEMENTED WITH TEG

In recent years, several silicon-based TEG structures have been reported in the literature, where the active pillars are constructed from SiGe alloy or GeSn alloy, a group-IV approach consistent with the silicon PV.[16] In addition, thin-film TEG versions have been discussed as alternatives to the micro-pillars.[17] In both cases, the area of the TEG can be large, and our suggestion is that the TEG area can match the area of the solar cell or panel. That being assumed, then, we propose to use the GeSn TEG as a supplement to the Si PV. Figure 11 shows the hybrid or composite structure, in which the TEG front face is in thermal contact with the PV rear face and the TEG rear face is in ambient air, yielding a considerable temperature drop across the TEG as desired. In addition, the TEG literature reveals that the thermoelectric ZT figure of merit for the proposed group IV TEG increases as the front face temperature of the TEG goes above 300 K; for example, the $Ge_{0.86}Sn_{0.14}$ TEG with front face at 550 K offers ZT = 0.92 (Fig. 6 of Ref. 18).

The approach shown in Fig. 11 provides two combined sources of electric power and is thereby superior to the method shown in Fig. 2. To give some context, Li *et al.*[19] have proposed and analyzed a low-power laser-actuated GaAs-PV + TEG hybrid that is functionally similar to that proposed here. Leaving aside the laser, the literature reports that solar PV is enhanced by TEG.[20] Now, we quantify the laser-power-to-electric-power conversion efficiency of this hybrid. The hybrid system's efficiency is calculated as

$$\eta_{PV-TEG} = \eta_{PV} + \eta_{TEG}, \tag{7}$$

where the maximum value of η_{TEG} is given by[20]

$$\eta_{TEG}^{(\max)} = \frac{T_h - T_c}{T_h}\left(\frac{\sqrt{1+ZT}-1}{\sqrt{1+ZT}+\frac{T_c}{T_h}}\right), \tag{8}$$

where T_h and T_c represent the hot and cold temperatures, respectively. As in Table II, the input power density provided by the laser is either 19 013 or 19 388 W. Perfect heat transfer from PV to TEG is assumed in (7).

Table III summarizes the results for the PV diode supplemented by TEG, with TEG based upon the GeSn-on-Si platform. If we look at the hybrid output electric power for the $Ge_{0.86}Sn_{0.14}$ TEG, we find 203 W output at the 19 388 W input, a result that compares immediately with the result of 157 W for PV alone, mentioned in Table II. This means that hybrid gives up to 30% improvement in OE conversion. We say "up to 30%" because the hybrid (see Table III) with $Ge_{0.88}Sn_{0.12}$ TEG offers a 26% increase in the total electrical output. Because Table III refers to an individual 15.6 × 15.6 cm^2 PV-and-TEG cell, we shall now scale up the hybrid to the 5 × 5 array-of-cells "panel" discussed earlier for PV, and we shall then consider the resulting PV + TEG panel whose area is then 0.61 m^2, a factor-of-25 increase over Table III. If we then use the conservative estimate of a factor-of-20 increase in the output electric power, the hybrid panel will provide 20 × 203 W, or about 4000 W as compared to the 3000 W found for the PV-only panel.

Because the TEG panel is "expensive" (in some sense of the word), it is usually necessary to perform a "cost–benefit analysis" of the hybrid panel in order to determine whether the obtained increase in electric power is justified by the added costs of construction.

X. THE THERMO-RADIATIVE APPROACH

The TR diode definitely can be used during beaming to obtain useful amounts of electric power at its output terminals, but we have found that this approach is limited in the laser beaming context, and here are the details. Regarding direct laser-illumination of the TR, that is "forbidden" in the sense that band-to-band absorption reduces the TR conversion efficiency. Absorption would create an unwanted photocurrent flowing in opposition to the desired electric current. In other words, the photon-absorption current is a loss current reducing the output electric current. The TR approach is attained by adding layers in thermal contact with the front face of the TR cell. A reflective layer is deposited on the TR input face, together with a thick layer that absorbs the laser beam in order to attain temperature rise in that absorber, an elevated temperature that is immediately transferred to the TR body.

Assuming those layers, the question we are raising is whether the figure of merit η for TR is comparable to that given by the PV approach. The first question to be answered in the TR simulation is the temperature of the absorber layer as it pertains to the incoming infrared power density. To be definite, we shall assume that this absorber is monocrystalline silicon and shall then turn to the results shown in Fig. 6 above, which indicates the absorber temperature rising into the 380–420 K range for D_b = 10 000 W/m^2. Thus, we can quantify the TR body temperature with D_b. Next, we turn to the theoretical TR results of Strandberg[21] who plots the output electrical-power density at the TR maximum power point (MPP) as a function of the bandgap E_g of the semiconductor used in the TR diode (Fig. 9 of Ref. 21). Electrical output power density curves for TR body temperatures of 500, 750, and 1000 K are presented assuming a TR radiative-face temperature of 300–400 K. Looking at that figure, we find that E_g must be in the range of 0.1–0.3 eV in order to get high W/m^2 electrical outputs. We also see that semiconductors with

17 May 2024 18:09:56

© Author(s) 2024

TABLE III. Summary of PV + TEG results based upon group IV.

TEG System	ZT at 550 (K)	Parameters: Efficiency ($\eta_{PV\text{-}TEG}$) T_h = 550 (K); T_c = 278 (K)	Parameters: Output electric power (W) for A = 0.0243 m^2
$Ge_{0.86}Sn_{0.14}$	0.92	0.42(d_{Si} = 180 μm); 0.43(d_{Si} = 500 μm)	194(d_{Si} = 180 μm); 203(d_{Si} = 500 μm)
$Ge_{0.88}Sn_{0.12}$	0.80	0.41(d_{Si} = 180 μm); 0.42(d_{Si} = 500 μm)	189(d_{Si} = 180 μm); 198(d_{Si} = 500 μm)

E_g > 1 eV give an extremely low output, orders of magnitude lower than that of narrow-gap materials, a result that rules out the use of silicon.

The group-IV alloy GeSn is an excellent choice for realizing the TR diode, and, in particular, we recommend the specific crystal alloy $Ge_{0.8}Sn_{0.2}$ in order to provide at a bandgap of E_g = 0.2 eV at an elevated temperature such as 550 K. In addition, it is essential to point out that this TR semiconductor will become segregated or unstable at TR body temperatures above 550 K. This then places an upper limit on the TR operation temperature.[21] In particular, we see in Ref. 21 an ideal TR output power density of 200 W/m^2 at 550 K. If we compare that density with our PV density result (Table II), we see that TR is 30× smaller, which is why PV is primary here.

XI. SYSTEM COSTS AND BENEFITS

The directed-energy system costs include maintenance costs, the capital cost of the laser, the cost of fueling or "powering" the laser, the cost of moving the laser (by mounting it on a truck, for example), the costs of the laser-aiming system (including real-time tracking when the energy beaming is required for moving systems), the costs of the PV cell, and the cost of its associated electrical circuitry. We are not saying that these costs are low. In fact, the overall cost could be high. We are saying that paying the total cost will be justified in most cases by the unique and valuable capabilities of the new electrification system. The benefits of the system will make the financial investment worthwhile.

XII. III–V SEMICONDUCTOR PHOTOVOLTAICS

We wish to present a wider context for our silicon-solar approach by detailing the excellent progress that has been made on III–V semiconductor photovoltaic cells during the past several years. A series of experiments on InGaAs, InGaAsP, GaAs, and GaSb PV devices, both single-junction and multi-junction devices, has proven the value of these devices for harvesting electric power from the beam of a Nd:YAG laser emitting at the 1064-nm wavelength.[22–27] The laser beam power incident upon the converter was in the range of 0.5–4 W CW. The optical input power of up to 50 W CW from a 980-nm diode laser was also investigated using III–Vs. By selecting their 300 K bandgaps to be below 1.12 eV (Si E_g), it is clear that the InGaAs and InGaAsP PVs will quite successfully convert the laser beam from the Yb-doped-fiber lasers and direct-diode lasers that are targeted in this paper. Therefore, the III–Vs definitely provide an alternative to silicon in the beaming system.

Regarding the power conversion efficiency (PCE) of the InGaAs PV at 1064 nm, two authors have projected that PCE decreases significantly as the PV cell temperature is increased to 373 K. The efficiency's rate-of-decrease is shown in Fig. 5 of Ref. 22 and in Fig. 7(d) of Ref. 24. Extrapolating the InGaAs cell temperature to 550 K, we find the PCE falling to 16% for the multi-junction device.[22]

To assist the "choice of semiconductor" for the PV device, we shall now sketch a silicon-to-III–V comparison by considering technical factors (such as thermal management during UHP illumination) and the manufacturing cost factors.

On a theoretical basis, we can compare the "thermal performance" of the InGaAs PV panel to that of the Si PV panel, assuming for both panels the same illumination area, the same heat sink structure, the same 1075-nm laser operating wavelength, the same incident laser power such as 10 kW CW, and the same bandgap obtained by adjusting III–V alloy composition (giving similar-to-Si absorption spectra). We note that all the InGaAs PV cells reported thus far have an overall layered thickness of 10 μm or less, whereas the Si PN cell thickness is in the 180–500 μm range. Because the InGaAs panel is comparatively "thin," our thermal analysis projects that the III–V panel will settle at a higher steady-state temperature than the Si does. If that is correct, then if we impose the same maximum operating temperature T_m upon both panels, the III–V will reach that T_m at a laser power input that is less than that for Si; hence, the III–V gives a less electrical output than the Si offers.

Turning to the manufacturing and production of PV cells and PV panels, we note three factors: (1) the construction of the III–V PVs is generally more complex than that of Si PVs, (2) the PV cell size in the III–V case will be generally smaller than the Si cell size due to the smaller diameter of available InP and GaAs "substrate" wafers as compared to the Si wafer diameter, a fact that may make the III–V PV panel assembly more difficult, and (3) the various cost factors appear to be larger in the III–V case.

XIII. SUMMARY

In the Introduction, it is stated that the optimized electrical output occurs at a PV temperature well above room temperature, and this statement seems to contradict the well-known decrease in PV

17 May 2024 18:09:56

© Author(s) 2024

efficiency with increased temperature. However, there is no contradiction because the electric output is given by the *product* of the efficiency and the laser power inputted to the PV. In the present system, as the PV temperature rises up from 293 K toward 600 K, the rate of laser power increase is slightly larger than the rate of efficiency decrease, and for that reason, the electric output power is maximum at the maximum allowed temperature.

We can outline the contribution of this paper by noting that this paper proposes, and gives quantitative theoretical analysis of, a novel laser-driven optical-to-electrical "power by light" system in which the innovative components of the system work together in a synergistic way to produce considerable electric power at a remote location. The multi-kilowatt electrical outputs that are predicted are based upon thermal, optical, and electrical modeling-and-simulation. Eleven scenarios for practical application of the directed-energy beaming over kilometers distance with low loss through the atmosphere are presented. The novel aspects of the system are as follows: (1) utilization of ultra-high-power CW SWIR laser beams giving 20 kW of power, (2) silicon photovoltaic OE conversion cells that are commercial solar cells "repurposed" for UHP monochromatic light, (3) large-area panels comprised of horizontally interconnected PV cells that "harvest" effectively after reaching a stable panel temperature during 20 kW/m^2 illumination by a collimated beam, (4) passive heat sinking of the panel instead of an electrically powered heat sink that deploys blowers and pumped liquids, (5) operation of PV cells and panels at elevated temperatures around 550 K, as discussed above, (6) series electrical connection of all cells in the panel to ensure full undiminished electrical output, (7) comparative analysis of thermo-radiative cells for beam conversion, (8) proposed panels comprised of hybrid PV + TEG modules for enhanced electrical output, and (9) a comparison of the Si PV converter with the InGaAs and InGaAsP photovoltaic approaches, suggesting that thermal management of the III–V PVs is problematic.

We can also sketch the strengths and weaknesses of the present system as compared to existing systems in the literature. The present strengths are as follows: (1) the proposed system builds upon widely proven and widely adopted solar panel technology, (2) the system builds upon widely proven UHP laser technology, and (3) the scope of potential practical applications is wide. The weaknesses are listed as follows: (1) the system cost is high; (2) the overall energy efficiency might be low when the energy needed to supply the laser is taken into account; (3) there are eye safety issues at the sending and receiving stations; (4) the beaming could be interrupted by smog, fog, smoke, and rain; (5) a pair of lenses is required at the laser station to form the collimated beam with the desired diameter; and (6) the high-temperature array might present some danger of burns or fire. It is important to note that all six of these factors are not specific to our system. They are six generic aspects that apply to any UHP beaming system, which means that these weaknesses are anticipated regardless of the hardware that is used for the PV panel, the laser supply, the laser-directing apparatus, etc.

Compared to existing power-by-light systems, the present system handles beam powers that are three orders-of-magnitude higher than those of existing systems. In addition, in most existing systems, the beam is focused to a spot on the PV converter, with the spot having a diameter of a few centimeters.

XIV. CONCLUSIONS

We have presented potential applications of UHP CW laser beaming to distant places where the harvesting of that beam by a semiconductor photodetector provides considerable electric power, power that is beneficial to various users and to society generally. In principle, a thermo-radiative (TR) diode could be employed for harvesting, but our studies indicate a TR electrical output that is much lower than that provided by a photovoltaic (PV) cell, thereby making PV the primary means.

For the UHP Yb-doped 1075-nm fiber laser, it is a fortuitous coincidence that the silicon solar cell is an ideal optical-to-electrical converter and that the cell can be a well-known commercial cell. Because the laser beam can be delivered through the atmosphere with very low loss, and because the collimated beam can have a diameter of around 1 m, a silicon solar-cell "panel" can be deployed for efficient harvesting. We have performed here a series of thermal and optical simulations that quantify the performances that can be expected, for example, performance using a monocrystalline silicon layer of thickness in the 180–500 μm range. Our results indicate that 500 μm is better than 180 μm, but not much better. Our results also predict about 15% OE conversion in the laser power range of 10–20 kW, with panel temperature in the 436–560 K range—in particular, an electrical output of 3000 W from a 0.6 m^2 panel illuminated by 20 kW 1075-nm beam, where the panel operates at a temperature of 550 K.

To obtain an additional electrical power output, the PV cell can be supplemented by a TEG cell whose area matches the PV area, and this hybrid uses thermal contact between the PV rear face and the TEG front face.

17 May 2024 18:09:56

ACKNOWLEDGMENTS

R.S. acknowledges the support of the U.S. Air Force Office of Scientific Research under Grant No. FA9550-21-1-0347. O.M. acknowledges the support from NSERC Canada (Discovery, SPG, and CRD Grants), Canada Research Chairs, Canada Foundation for Innovation, Mitacs, PRIMA Québec, Defence Canada (Innovation for Defence Excellence and Security, IDEaS), the European Union's Horizon Europe research and innovation program under Grant Agreement No. 101070700 (MIRAQLS), the U.S. Army Research Office under Grant No. W911NF-22-1-0277, and the U.S. Air Force Office of Scientific and Research under Grant No. FA9550-23-1-0763.

AUTHOR DECLARATIONS

Conflict of Interest

The authors have no conflicts to disclose.

Author Contributions

Richard Soref: Conceptualization (lead); Project administration (equal); Supervision (equal); Writing – original draft (lead); Writing – review & editing (equal). **Francesco De Leonardis**: Conceptualization (supporting); Formal analysis (lead); Software (lead);

© Author(s) 2024

Writing – original draft (supporting); Writing – review & editing (equal). **Gerard Daligou**: Formal analysis (supporting); Writing – review & editing (equal). **Oussama Moutanabbir**: Conceptualization (supporting); Project administration (equal); Supervision (equal); Writing – review & editing (equal).

DATA AVAILABILITY

The data that support the findings of this study are available within the article.

REFERENCES

[1] C. Algora, I. Garcia, M. Delgado, R. Pena, C. Vazquez, M. Hinojosa, and I. Rey-Stolle, "Beaming power: Photovoltaic laser power converters for power-by-light," Joule **6**, 340–368 (2022).
[2] H. Haas, J. Elmirghani, and I. White, "Optical wireless communication," Philos. Trans. R. Soc., A **378**, 20200051 (2020).
[3] Trumpf GMBH, TruFlow series, 20 kW CW output CO_2 lasers emitting at 10 600 nm.
[4] Laserline GMBH, LDF series, 20 kW CW output from stacks of direct-diode bars emitting in the 900 nm to 1080 nm range.
[5] Coherent, DD series, 10 kW CW output, direct-diode lasers emtting at 967 nm.
[6] Raycus, 10 kW CW output, direct-diode laser emitting at 910 nm.
[7] IPG Photonics, ELS 4000 series, 4 kW CW output from Er-doped-fiber laser emitting at 1567 nm.
[8] K. Ludewigt, A. Liem, U. Stuhr, and M. Jung, "High-power laser development for laser weapons," Proc. SPIE **11162**, 1116207 (2019).
[9] J. Sun, L. Liu, L. Han, Q. Zhu, X. Shen, and K. Yang, "100 kW ultra high power fiber laser," Opt. Continuum **1**(9), 1932 (2022).
[10] IPG Photonics, YLS series, 20 kW CW output from Yb-doped-fiber laser emitting at 1075 nm center wavelength with 10-nm spectral width.
[11] A. Berk, P. Conforti, R. Kennett, T. Perkins, F. Hawes, and J. van den Bosch, "MODTRAN® 6: A major upgrade of the MODTRAN® radiative transfer code," in 2014 6th Workshop on Hyperspectral Image and Signal Processing: Evolution in Remote Sensing (WHISPERS), 24–27 June 2014.
[12] T. Saga, "Advances in crystalline silicon solar cell technology for industrial mass production," NPG Asia Mater. **2**(3), 96–102 (2010).
[13] J. Peng *et al.*, "Evolution of silicon wafer dimensions," J. Phys.: Conf. Ser. **2221**, 012025 (2022).
[14] K. Rajkanan, R. Singh, and J. Shewchun, "Absorption coefficient of silicon for solar cell calculations," Solid State Electron. **22**, 793–795 (1979).
[15] M. A. Green, J. Zhao, A. Wang, and S. R. Wenham, "45% efficient silicon photovoltaic cell under monochromatic light," IEEE Electron Device Lett. **13**(6), 317 (1992).
[16] D. Vashaee, "SiSn and SiGeSn—Promising thermoelectric materials," in AFRL Workshop, Dayton, OH, 17–18 September 2019.
[17] M. Kurosawa and O. Nakatsuka, "Thermoelectric properties of tin-incorporated group-IV thin films," ECS Trans **104**(4), 183 (2021).
[18] D. Spirito, N. von den Driesch, C. Manganelli, M. Zoellner, A. Corley-Wiciak, Z. Ikonic, T. Stoica, D. Grutzmacher, D. Buca, and G. Capellini, "Thermoelectric efficiency of epitaxial GeSn alloys for integrated Si-based applications: Assessing the lattice thermal conductivity by Raman thermometry," ACS Appl. Energy Mater. **4**, 7385–7392 (2021).
[19] Y. Li, Z. Zhang, H. Zhang, Z. Xiao, L. Luming, and P. Jiang, "Numerical and experimental performance evaluation of a laser-concentrated photovoltaic-thermoelectric generator hybrid system," Opt. Express **30**(11), 19465 (2022).
[20] R. Chandel, S. Singh Chandel, D. Prasad, and R. Prakash Dwivedi, "Review on thermoelectric systems for enhancing photovoltaic power generation," Sustainable Energy Technol. Assess. **53**, 102585 (2022).
[21] R. Strandberg, "Theoretical efficiency limits for thermoradiative energy conversion," J. Appl. Phys. **117**, 056105 (2015).
[22] J. Yin, Y. Sun, A. Wang, S. Yu, J. Wang, Q. Fu, J. Qin, Y. Han, W. Zhang, S. Zhang, C. Xue, and J. Dong, "High-voltage 1064 nm InGaAsP multijunction laser power converters," IEEE Electron Device Lett. **43**, 1291–1294 (2022).
[23] S. Fafard and D. Masson, "Perspective on photovoltaic optical power converters," J. Appl. Phys. **130**, 160901 (2021).
[24] Y. Gou, H. Wang, J. Wang, Y. Zhang, R. Niu, X. Chen, B. Wang, Y. Xiao, Z. Zhang, W. Liu, H. Yang, and G. Deng, "1064 nm InGaAs metamorphic laser power converts with over 44% efficiency," Opt. Express **30**, 42178–42185 (2022).
[25] S. Fafard and D. Masson, "High-efficiency and high-power multijunction InGaAs/InP photovoltaic laser power converters for 1470 nm," Photonics **9**, 438 (2022).
[26] N. A. Kalyuzhnyy, V. Emelyanov, V. Evstropov, S. Mintairov, M. Mintairov, M. Nahimovich, R. Salii, and M. Shvarts, "Optimization of photoelectric parameters of InGaAs metamorphic laser (λ = 1064 nm) power converters with over 50% efficiency," Sol. Energy Mater. Sol. Cells **217**, 110710 (2020).
[27] J. Yin, Y. Sun, S. Yu, Y. Zhao, R. Li, and J. Dong, "1064 nm InGaAsP multijunction laser power converters," J. Semicond. **41**, 062303 (2020).

17 May 2024 18:09:56

© Author(s) 2024